Materials Science & Engineering C 117 (2020) 111294

Contents lists available at ScienceDirect

Materials Science & Engineering C

journal homepage: www.elsevier.com/locate/msec

Injectable *in situ* forming thermo-responsive graphene based hydrogels for cancer chemo-photothermal therapy and NIR light-enhanced antibacterial applications

Rita Lima-Sousa[a], Duarte de Melo-Diogo[a,*], Cátia G. Alves[a], Cátia S.D. Cabral[a], Sónia P. Miguel[a,b], António G. Mendonça[a,c], Ilídio J. Correia[a,d,*]

[a] CICS-UBI – Centro de Investigação em Ciências da Saúde, Universidade da Beira Interior, 6200-506 Covilhã, Portugal
[b] CPIRN-IPG – Centro de Potencial e Inovação de Recursos Naturais, Instituto Politécnico da Guarda, 6300-559 Guarda, Portugal
[c] Departamento de Química, Universidade da Beira Interior, 6201-001 Covilhã, Portugal
[d] CIEPQPF – Departamento de Engenharia Química, Universidade de Coimbra, 3030-790 Coimbra, Portugal

ARTICLE INFO

Keywords:
Antibacterial activity
Cancer
Chemo-photothermal therapy
Graphene family nanomaterials
Injectable hydrogel

ABSTRACT

Functionalized graphene oxide (GO) and reduced GO (rGO) based nanomaterials hold a great potential for cancer photothermal therapy. However, their systemic administration has been associated with an accelerated blood clearance and/or with suboptimal tumor uptake. To address these limitations, the local delivery of GO/rGO to the tumor site by 3D matrices arises as a promising strategy. In this work, injectable chitosan-agarose *in situ* forming thermo-responsive hydrogels incorporating GO (thermogel-GO) or rGO (thermogel-rGO) were prepared for the first time. The hydrogels displayed suitable injectability and gelation time, as well as good physicochemical properties and cytocompatibility. When irradiated with near infrared (NIR) light, the thermogel-rGO produced a 3.8-times higher temperature increase than thermogel-GO, thus decreasing breast cancer cells' viability to 60%. By incorporating an optimized molar ratio of the Doxorubicin:Ibuprofen combination on thermogel-rGO, this formulation mediated a chemo-photothermal effect that further diminished cancer cells' viability to 34%. In addition, the hydrogels' antibacterial activity was further enhanced upon NIR laser irradiation, which is an important feature considering the possible risk of infection at the site of administration. Overall, thermogel-rGO is a promising injectable *in situ* forming hydrogel for combinatorial chemo-photothermal therapy of breast cancer cells and NIR light enhanced antibacterial applications.

1. Introduction

During this last decade, 2D nanomaterials (*e.g.* black phosphorus nanostructures [1–6], Boron nanosheets [7], Antimonene-based nanomaterials [8–10], MXene [11,12]) have emerged in different fields. In particular, the unique physicochemical, optical and mechanical properties of graphene oxide (GO) and reduced graphene oxide (rGO) have propelled their use in different biomedical applications, such as cancer photothermal therapy (PTT) [13–19]. These materials are capable of absorbing near infrared (NIR) light, producing a temperature increase upon irradiation that can ablate the cancer cells [20–22]. In this regard, rGO displays a higher photothermal capacity than GO, due to its improved NIR absorption [22].

Despite their photothermal capacity, as-synthesized GO and rGO are rapidly cleared from circulation, hindering their ability to passively accumulate at the tumor site [14]. To overcome this drawback, GO and rGO have been functionalized with poly(ethylene glycol) (PEG) derivatives [23–26]. Nevertheless, recently it was uncovered that anti-PEG antibodies are produced after the intravenous administration of PEGylated graphene derivatives, which in turn mediate the rapid clearance of this material from the blood circulation in subsequent injections (known as the accelerated blood clearance phenomenon) [27]. Such is further aggravated by the fact that an exhaustive literature analysis just unveiled that less than 1% of the injected nanomaterials' dose reaches the tumor [28]. In this way, the development of new GO/rGO delivery strategies capable of overcoming the limitations associated with the systemic administration of these nanomaterials is of upmost importance.

The local delivery of GO/rGO at the tumor site by 3D matrices is a promising strategy to enhance the therapeutic potential of these

* Corresponding authors.
E-mail addresses: demelodiogo@fcsaude.ubi.pt (D. de Melo-Diogo), icorreia@ubi.pt (I.J. Correia).

https://doi.org/10.1016/j.msec.2020.111294
Received 21 February 2020; Received in revised form 6 July 2020; Accepted 21 July 2020
Available online 24 July 2020
0928-4931/

nanomaterials. For instance, we have previously demonstrated that 3D printed scaffolds' properties are enhanced by incorporating GO and rGO in the scaffolds' matrices [29,30]. However, for a cancer related application, a 3D matrix incorporating GO/rGO should be administrable at the tumor site using a minimally invasive procedure with reduced risk of infection [31–33]. In this context, injectable hydrogels exhibiting *in situ* gelation capabilities hold a great potential for mediating a tumor-confined delivery of GO/rGO with minimal systemic exposure [32]. So far, the majority of the prepared injectable hydrogels containing GO or rGO are based on synthetic polymers (*e.g.* poly(*N*-isopropylacrylamide), polyethylenimine and poloxamers) [34,35]. However, the use of natural polymers for preparing the injectable hydrogels is far more attractive, since these display an improved biocompatibility/degradability and may introduce additional functionalities such as antibacterial activity or thermo-responsive gelation [36–38]. In this way, the formulation of natural polymer-based injectable hydrogels incorporating GO/rGO opens a venue for the preparation of multifunctional systems that can be applied for cancer photothermal therapy, NIR-enhanced drug delivery and antibacterial activity.

In this work, injectable chitosan-agarose *in situ* forming thermo-responsive hydrogels incorporating GO (thermogel-GO) or rGO (thermogel-rGO) were prepared for the first time. Chitosan was chosen due to its antibacterial activity, while agarose was selected due to its ability to mediate a thermo-responsive gelation [39–43]. The hydrogels displayed suitable injectability and gelation time, as well as good physicochemical properties and cytocompatibility. When irradiated with NIR light, the thermogel-rGO was able to produce a 3.8-times higher temperature increase than thermogel-GO due to the increased photothermal capacity or rGO. Consequently, the PTT mediated by thermogel-rGO could decrease breast cancer cells' viability to 60%, while that induced by thermogel-GO only reduced to 73%. By incorporating an optimized molar ratio of the Doxorubicin:Ibuprofen (DOX:IBU) combination on thermogel-rGO, this formulation mediated a chemo-photothermal effect that further diminished cancer cells' viability to 34%. The hydrogels' antibacterial activity, an important feature considering the possible risk of infection at the injection site, was also enhanced upon NIR laser irradiation.

2. Materials and methods

2.1. Materials

Agarose (low melting point-ultrapure grade) was obtained from Nzytech (Lisbon, Portugal). Chitosan (medium molecular weight), GO nanocolloids, Phosphate buffered saline (PBS), Dulbecco's modified Eagle's medium F-12 (DMEM-F12), penicillin/streptomycin, trypsin, resazurin and LB broth were purchased from Sigma Aldrich (Sintra, Portugal). L-ascorbic acid was bought from Fisher Scientific (Oeiras, Portugal). Acetic acid was acquired from Pronalab (Barcelona, Spain) and lysozyme from chicken egg was purchased from Alfa Aesar (Haverhill, MA, USA). Michigan cancer foundation-7 (MCF-7) cell line was obtained from ATCC (Middlesex, UK). Normal human dermal fibroblasts (NHDF) were acquired from Promo-Cell (Heidelberg, Germany). Fetal bovine serum (FBS) was bought from Biochrom AG (Berlin, Germany). *Staphylococcus aureus* clinical isolate (*S. aureus*; ATCC 25923) and *Escherichia coli* DH5a (*E. coli*) were used to evaluate the antimicrobial properties. Doxorubicin was acquired from Carbosynth (Berkshire, UK). Ibuprofen was obtained from Tokyo Chemical Industry (Tokyo, Japan). Water used in all experiments was double deionized (0.22 μm filtered, 18.2 MΩ cm).

2.2. Methods

2.2.1. Preparation of the different hydrogels

The hydrogels based on agarose and chitosan were prepared by adapting a protocol previously described elsewhere [38]. Initially, different contents of agarose and chitosan were screened in order to disclose the conditions that yield hydrogels with adequate injectability and gelation time (Table S1). For such, a heated solution of agarose (dissolved in water) was mixed with a solution of chitosan (dissolved in 1% acetic acid solution). This agarose-chitosan solution (final volume of 1 mL) was then loaded into a syringe and extruded (200 μL *per* template) into hollow cylindrical and removable templates (⌀ = 8 mm; height = 4 mm) in order to attain hydrogels with uniform macroscopic features. To assess hydrogels' gelation time, the agarose-chitosan solution was also extruded to microtubes and the time required to achieve complete gelation was determined.

The best performing hydrogel formulation (prepared using 10 mg of agarose and 10 mg of chitosan in a final volume of 1 mL, termed as thermogel from here on) was selected to incorporate the graphene family nanomaterials. The hydrogels incorporating GO (thermogel-GO) were formulated by adding GO (50 μg) to the agarose-chitosan solution, prepared following the protocol described above. Similarly, the hydrogels incorporating rGO (thermogel-rGO) were formulated through the addition of environmentally friendly rGO (50 μg; attained by treating GO with 3 mM of L-ascorbic acid for 60 min at 80 °C [22]) to the agarose-chitosan solution. The gelation time of these hydrogels was determined as described above. For the remaining assays, these hydrogels were also assembled by using the hollow cylindrical molds (200 μL *per* template).

2.2.2. Characterization of the hydrogels

The swelling profile of the hydrogels was determined following a method described in the literature [38]. In brief, thermogel, thermogel-GO and thermogel-rGO were immersed in a PBS solution (pH 7.4) at 37 °C, under stirring. At predetermined intervals, the hydrogels were removed from the PBS solution, weighted and then immersed in a new PBS solution. The swelling ratio was determined using the following equation (W_t and W_i represent the final and initial weight of the gels, respectively):

$$\text{Swelling Ratio}\ (\%) = \left(\frac{W_t - W_i}{W_i}\right) \times 100 \quad (1)$$

Hydrogels' degradation profile was studied by incubating each hydrogel in a PBS solution (pH 7.4; 10 mL) containing Lysozyme (13.6 mg/L), at 37 °C, under stirring for 14 days [30]. Throughout the assay, the PBS-enzyme solution was replaced twice a day. At predetermined time points, the hydrogels were recovered, rinsed with water, freeze-dried and then weighted. The weight loss at the given times was calculated having into account the following equation (W_i and W_t represent the hydrogels' initial weight and the hydrogels' weight at time t, respectively):

$$\text{Weight loss}\ (\%) = \left(\frac{W_i - W_t}{W_i}\right) \times 100 \quad (2)$$

The photothermal capacity of thermogel, thermogel-GO and thermogel-rGO was assessed by following a protocol described elsewhere [22]. In brief, the different gels were immersed in water, and then were exposed to NIR light (808 nm, 1.7 W/cm^2) over a period of 10 min. The temperature changes were monitored using a thermocouple thermometer. Water was used as control. Additionally, Scanning Electron Microscopy (SEM) images of the different hydrogels were taken to analyze the hydrogels' morphology (acceleration voltage of 20 kV using a Hitachi S-3400N scanning electron microscope (Japan)).

The rheological characterization was carried out in a Thermostated Brookfield DV3T cone-plate rheometer using a CP52Z or CP40Z cone (Brookfield Ametek, Massachusetts, USA), with a sample volume of 0.5 mL [44]. The viscosity of the samples was assessed at 25 °C at increasing speeds (20–250 rpm). For the thixotropic behavior test, the samples were subjected to an increase and immediate decrease in the shear rates (80 to 500 s^{-1}). To assess the thermo-responsiveness, the

samples' viscosity at various temperatures was measured at a constant shear rate (80 s^{-1}). For all assays, the results were not considered for the analysis if the torque value was superior to 95%.

For analyzing the long-term stability of the hydrogels, these were formulated and stored at 4 °C, during 7 days. Afterwards, the formulations were re-heated and their re-injectability and re-gelification were evaluated.

2.2.3. Evaluation of hydrogels' cytocompatibility

The cytocompatibility of the hydrogels was assessed against MCF-7 cells and NHDF using the resazurin method [45]. For the cell culture assays, both cell lines were cultured in DMEM-F12 supplemented with 10% (v/v) of FBS and 1% (v/v) of penicillin/streptomycin in a humidified incubator (37 °C, 5% CO_2). In brief, 2×10^4 cells/well were seeded in 12-well plates. After 24 h, the medium was changed and cells were incubated with the thermogel, thermogel-GO and thermogel-rGO for 24 and 48 h. Afterwards, the medium was replaced with fresh cell culture medium containing 10% (v/v) of resazurin, and the cells were incubated for another 4 h in the dark (37 °C, 5% CO_2). Then, the cells' viability was determined by analyzing the fluorescence of resorufin (λ_{ex} = 560 nm; λ_{em} = 590 nm) in a Spectramax Gemini EM spectrofluorometer (Molecular Devices LLC, CA, USA). Non-treated cells and cells incubated with ethanol (70% (v/v)) were used as the negative (K^-) and positive (K^+) controls, respectively.

2.2.4. Determination of hydrogels' NIR light-enhanced antibacterial activity

The NIR light-enhanced antibacterial activity of the gels was determined against *Staphylococcus aureus* (*S. aureus*) and *Escherichia coli* (*E. coli*), gram-positive and gram-negative bacterium, respectively, *via* an agar diffusion method as reported elsewhere [30]. Briefly, 200 μL of bacteria in growth medium, at a concentration of 1×10^8 Colony-Forming Unit (CFU)/mL, were distributed onto an agar plate. Afterwards, 3 samples of the various hydrogels were placed onto the agar cultured with the bacteria. After 4 h of incubation at 37 °C, the hydrogels were irradiated with NIR light (808 nm, 1.7 W/cm^2, 10 min). Upon reaching 24 h of incubation, photographs of the hydrogels were taken, and the diameters of the inhibition halos were measured by using the ImageJ software (National Institutes of Health). To investigate bacteria growth at the hydrogels' surface, these were analyzed by SEM.

2.2.5. Evaluation of hydrogels' photothermal therapy towards breast cancer cells

The photothermal therapy mediated by the hydrogels towards breast cancer cells was assessed as previously described by our group with slight adjustments [46]. For such, MCF-7 cells were seeded as described in Section 2.2.3. and were incubated with the thermogel-GO (10 μg/mL of GO) and thermogel-rGO (10 μg/mL of rGO). After 4 h of incubation, the hydrogels were irradiated with NIR light (808 nm, 1.7 W/cm^2) for 10 min. Upon reaching 24 h of incubation, the cells' viability was determined using the resazurin method as described in Section 2.2.3.

2.2.6. Combinatorial chemo-photothermal therapy mediated by thermogel-rGO incorporating DOX and IBU

First, the optimal DOX:IBU combination towards MCF-7 cells was determined in order to be incorporated on the thermogel-rGO formulation (described in detail in the Supporting information). Then, the thermogel-rGO precursor solutions were prepared as described in Section 2.2.1, and the 1:5 molar ratio of the DOX:IBU combination was incorporated into the polymeric matrix. The DOX and IBU release from thermogel-rGODI(2x) was evaluated by placing this formulation in contact with a PBS solution (pH 7.4) containing lysozyme (13.6 mg/L) at 37 °C. At pre-determined time points, the solution was recovered and replaced with a fresh PBS-lysozyme solution. Then, the content of DOX and IBU in the recovered solutions was determined by absorption spectroscopy [47].

For the determination of the combinatorial chemo-photothermal therapy mediated by the hydrogels, MCF-7 cells seeded as described in the Section 2.2.3. were incubated with thermogel-rGODI(1x) (10 μg/mL of rGO; 45.2 μM of the DOX:IBU 1:5 combination) or thermogel-rGODI (2x) (10 μg/mL of rGO; 90.4 μM of the DOX:IBU 1:5 combination). After 4 h of incubation, cells were irradiated with NIR light (as described in Section 2.2.5.). Finally, upon reaching 24 h of incubation time, cells' viability was determined using the resazurin assay as described in Section 2.2.3.

2.2.7. Statistical analysis

A One-way analysis of variance (ANOVA) with the student-Newman-Keuls test was employed in multiple group comparisons. A *p*-value lower than 0.05 ($p < 0.05$) was considered statistically significant. All data are represented as the mean ± standard deviation (SD). The software GraphPad Prism v6.0 (Trial version, GraphPad Software, CA, USA) was used for data analysis.

3. Results and discussion

3.1. Preparation and characterization of the injectable in situ forming thermo-responsive hydrogels

Initially, different contents of agarose to chitosan were screened for the preparation of the injectable *in situ* forming thermo-responsive hydrogels (please see Table S1). The different agarose-chitosan solutions were loaded into syringes and the resistance to extrusion (injectability) was evaluated. This is of extreme importance since solutions must be easily extruded to avoid any discomfort to patients [48]. Simultaneously, the time required for the solutions to form a gel was assessed. This transition from liquid to a gel state is mediated by the thermo-responsive behavior of agarose. From the different polymeric solutions produced, the one prepared using 10 mg of agarose and 10 mg of chitosan displayed good injectability and gelation time - Table S1 (the gel attained using this polymeric mixture is termed as thermogel from here on).

Therefore, this polymeric formulation (10 mg of agarose + 10 mg of chitosan) was selected to be loaded with GO and rGO, yielding thermogel-GO and thermogel-rGO, respectively. As importantly, the addition of these graphene family nanomaterials to the gels did not affect their gelation time nor their injectability (Fig. 1A). In fact, all the three formulations attained gelation after 10 min (Fig. 1A). For the subsequent studies, individual gels were assembled by dispersing their respective polymeric solutions (200 μL *per* template) into cylindrical molds in order to obtain thermogel, thermogel-GO and thermogel-rGO with similar and uniform macroscopic characteristics (Fig. S1). The analysis of the hydrogels' cross-section structure by SEM revealed that these display a highly porous interconnected inner structure (Fig. S1). Interestingly, the thermogel-GO and thermogel-rGO presented a uniform and well-ordered network, which could result from the GO/rGO capacity to improve structures' mechanical properties [29,30].

Then, the swelling behavior of the hydrogels was investigated (Fig. 1B). The three hydrogels exhibited similar swelling profiles, with all the formulations reaching a maximum swelling that averages 24% after 45 min of incubation (Fig. 1B). Afterwards, the swelling stabilized. Such feature is crucial since an abrupt or high swelling would compromise the possible intratumoral application of the gels. This swelling behavior is also in line with that of other injectable chitosan or agarose-based hydrogels reported in the literature [49–51].

Then, the degradability of the hydrogels in biological-mimicking conditions was investigated (Fig. 1C). In general, all the formulations displayed an increased weight loss within the first day of incubation (Fig. 1C). The weight loss of all the formulations were around 48–56% after 14 days of degradation, thereby demonstrating a suitable degradability for the aimed biomedical application. These degradation behaviors are in agreement with that of other chitosan-based hydrogels

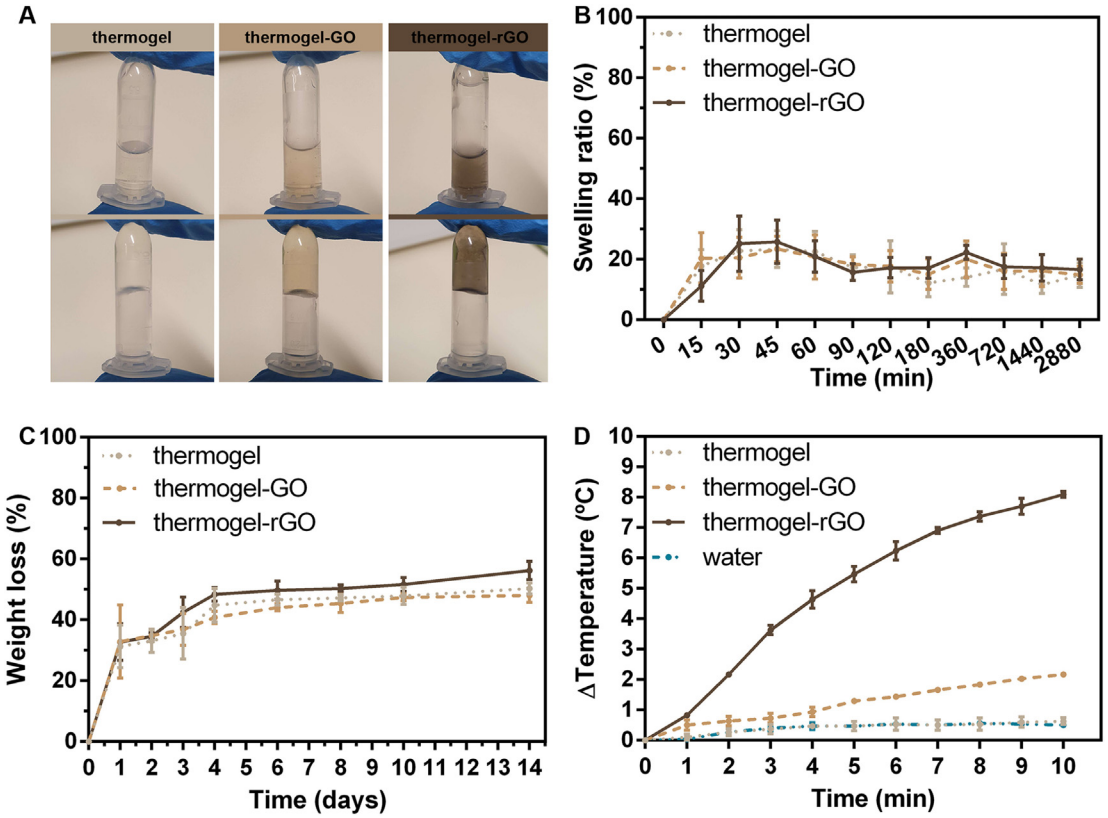

Fig. 1. Characterization of the physicochemical properties of the injectable *in situ* forming hydrogels. Macroscopic images of the thermogel, thermogel-GO and thermogel-rGO gelation (A). Evaluation of the hydrogels' swelling capacity over a period of 48 h (B). Determination of hydrogels' weight loss over a period of 14 days (C). Temperature variation curves of the different hydrogel formulations during 10 min of irradiation (808 nm, 1.7 W/cm^2) (D). Data represent mean ± SD, n = 3.

[52]. As importantly, the hydrogels' biodegradation may enable their application for therapeutics' delivery [36,52].

The rheological curves (Fig. S2A) revealed that the viscosity of all the hydrogels decreases with an increase in the speed from 20 to 250 rpm, which indicates a non-Newtonian, shear thinning behavior [44,53]. Furthermore, thermogel, thermogel-GO and thermogel-rGO demonstrated a thixotropic behavior (Fig. S2B), meaning that the hydrogels become less viscous if a shear stress is applied and that then they recover the solid form [54,55]. Additionally, the viscosity of the hydrogels was influenced by the temperature, indicating their thermo-responsive assembly (Fig. S2C).

Then, the stability of thermogel, thermogel-GO and thermogel-rGO was analyzed (Fig. S3). All the formulations maintained their injectability and thermo-responsive gelification even after storage at 4 °C for 7 days and subsequent re-heating, hence demonstrating a good long-term stability (Fig. S3).

Subsequently, the photothermal capacity of the gels was determined. The exposure of thermogel-GO to NIR light (808 nm, 1.7 W/cm^2) during a period of 10 min generated a temperature increase of about 2.2 °C (Fig. 1D). In stark contrast, the thermogel-rGO produced a temperature increase of about 8.1 °C (Fig. 1D). Such is in agreement with the higher NIR absorption displayed by rGO in comparison to GO [22]. Attaining such temperature increases is of paramount importance since it can induce damage to cancer cells [56]. As expected, the irradiation of the thermogel did not cause a meaningful temperature increase, since this formulation does not have any photothermal agent within its matrix (Fig. 1D). Water (control) exposed to NIR light did also not suffer any meaningful temperature increase, which is in agreement with its weak/minimal interaction with 808 nm light [57]. The photothermal capacity of thermogel-rGO is in line with that of hyaluronic acid-functionalized rGO previously synthesized by our group, suggesting that the incorporation of rGO in the hydrogels' matrix does not impair its photothermal capacity (8.1 °C *vs.* 10.7 °C at a concentration of 10 μg/mL of rGO) [22]. In another work, injectable PEG-thiol-palladium nanosheets hydrogels produced a temperature increase of about 11 °C, but required a higher content of photothermal agent (60 μg/mL of palladium nanosheets) [58]. These facts highlight the potential of thermogel-rGO for photothermal therapy.

Finally, the cytocompatibility of the different hydrogels towards MCF-7 cells (breast cancer cell model) and NHDF (healthy cells) was investigated. Both cell lines incubated with the thermogel, thermogel-GO and thermogel-rGO remained highly viable (> 72% cell viability), thus suggesting the cytocompatible profile of these materials (Fig. 2). As importantly, the viability of cells incubated with thermogel-GO and thermogel-rGO was similar to those incubated with thermogel. These results indicate that the incorporation of GO and rGO within the hydrogels' polymeric matrix does not impair the hydrogels' cytocompatibility.

Taken together, these results show that the thermogel-GO and thermogel-rGO display suitable physicochemical, optical and biological properties to be explored as *in situ* forming injectable matrices for NIR-responsive biomedical applications.

3.2. Hydrogels' NIR-light enhanced antibacterial activity

The local administration of *in situ* forming hydrogels can be performed using a minimally invasive procedure [31]. Nevertheless, it still carries some risk of infection at the injection site, demanding the use of antibiotics [31].

Considering that the hydrogels contain chitosan in their composition, and that it has been widely described as an antibacterial agent [59], the hydrogels' possible antibacterial activity against *S. aureus* and *E. coli* (gram-positive and gram-negative bacteria, respectively) was investigated *via* an agar diffusion method. The inhibition area induced

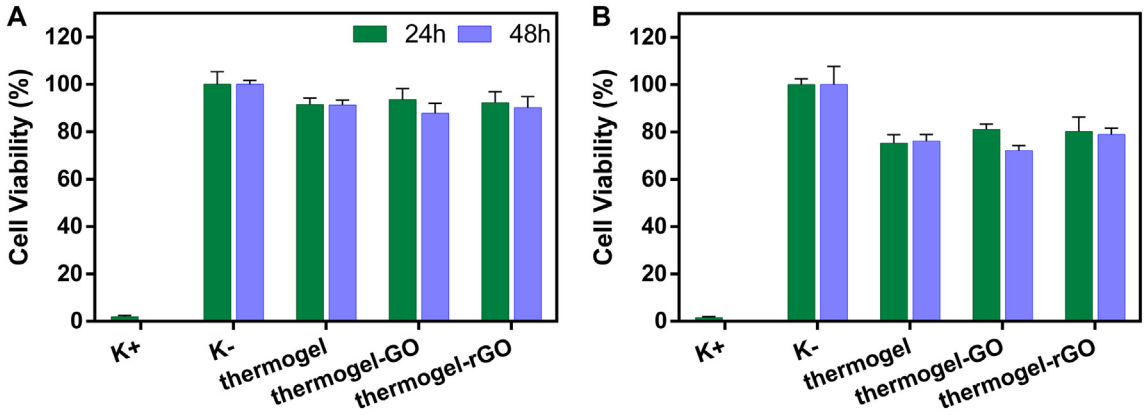

Fig. 2. Cytocompatibility of thermogel, thermogel-GO and thermogel-rGO towards MCF-7 (A) and NHDF (B) cells after 24 and 48 h of incubation. Data represent mean ± SD, n = 5. K^- and K^+ represent negative and positive controls, respectively.

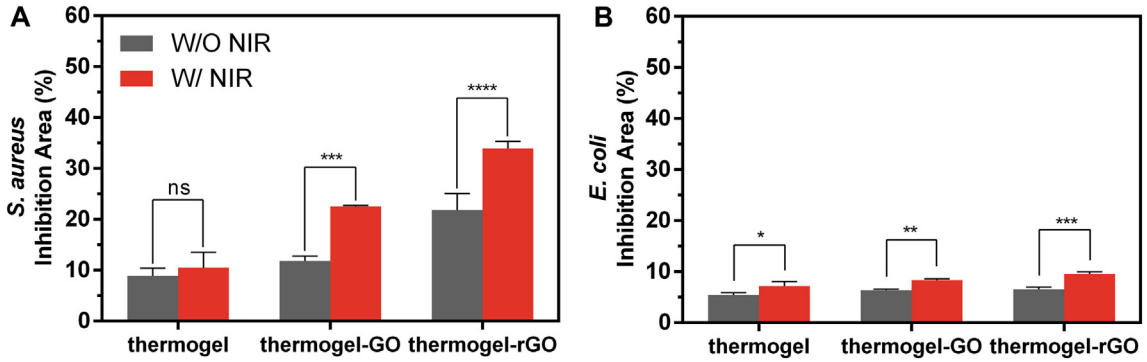

Fig. 3. Characterization of the NIR-light enhanced antibacterial activity of the different hydrogel formulations. Analysis of the inhibition area obtained for thermogel, thermogel-GO and thermogel-rGO in contact with *S. aureus* (A) or *E. coli* (B) without NIR (W/O NIR) or with NIR (W/ NIR) laser irradiation (808 nm, 1.7 W/cm^2, 10 min). Values are presented as mean ± SD, n = 3. (*p < 0.05, **p < 0.01, ***p < 0.001, ****p < 0.0001, ns = non-significant).

by the thermogel, thermogel-GO and thermogel-rGO against *S. aureus* was superior to that attained in *E. coli* (Fig. 3A and B). Such is consistent with the fact that chitosan has a stronger antibacterial activity against gram-positive bacteria due to the absence of an outer lipid membrane [59,60]. Furthermore, the irradiation of thermogel-GO and thermogel-rGO with NIR light (808 nm, 1.7 W/cm^2, 10 min) further increased their inhibitory activity (Fig. 3A and B). In particular, the inhibition area of thermogel-rGO towards *S. aureus* increased from 22 to 34% upon NIR laser irradiation (Fig. 3A). Such may be explained by the fact that the higher photoinduced heat generated by thermogel-rGO could enhance the chitosan dissolution from the hydrogels' polymeric matrix, leading to an improved effect. The SEM analysis is also consistent with these results since fewer bacterial populations were found at the surface of the thermogel-GO and thermogel-rGO exposed to NIR light (Fig. S4). Taken together, these results indicate that the thermogel-rGO can be explored for NIR-light enhanced antibacterial applications.

3.3. Hydrogels' photothermal therapy towards breast cancer cells

After confirming the cytocompatibility of the thermogel-GO and thermogel-rGO (Section 3.1.), their phototherapeutic capacity towards breast cancer cells was investigated. For such, MCF-7 cells were incubated with these formulations and then exposed to NIR light (808 nm, 1.7 W/cm^2, 10 min) - Fig. 4A. The combined action of thermogel-GO and NIR light decreased MCF-7 cells' viability from 93 to 73% (Fig. 4B). In contrast, cells' viability was further decreased from 92 to 60% when these were treated with the thermogel-rGO plus NIR light (Fig. 4B). The enhanced therapeutic effect induced by thermogel-rGO upon NIR laser irradiation is consistent with its higher photothermal capacity (Fig. 1D). As importantly, cells solely treated with NIR light remained highly viable (Fig. 4B). Such result is in agreement with low/minimal interactions of NIR light with biological components [61,62]. Furthermore, these results also attest that thermogel-rGO can produce an improved on-demand phototherapeutic effect upon NIR laser irradiation.

Jiang and coworkers prepared a PEG-thiol-palladium nanosheets hydrogel that in combination with NIR light (808 nm, 0.6 W/cm^2, 10 min) decreased 4T1 cells' viability to about 54% [58]. Herein, thermogel-rGO plus NIR light (808 nm, 1.7 W/cm^2, 10 min) reduced cell's viability to about 60% but required a lower content of the photothermal agent (rGO: 10 μg *vs.* palladium nanosheets: 60 μg).

3.4. Chemo-PTT mediated by thermogel-rGO incorporating DOX and IBU

After confirming the enhanced photothermal capacity of thermogel-rGO, we investigated its ability to deliver a drug combination to cancer cells. The use of drug combinations for cancer therapy is appealing since these can act on multiple cancer hallmarks, overcoming drug resistance mechanisms [63]. In this way, the local administration of drug combinations through injectable hydrogels may overcome the problems associated with the intravenous administration of free drugs (*e.g.* low solubility and off-target toxicity), enabling an enhanced and safer therapeutic effect [32].

Initially the efficacy of different DOX:IBU molar combination ratios (from 5:1 to 1:5) towards MCF-7 cells was screened (Fig. S5). DOX was selected since it is commonly used in combination with other chemotherapeutic drugs (*e.g.* Sorafenib and Docetaxel) for cancer therapy [64,65]. IBU is a nonsteroidal anti-inflammatory drug that has potential to be used as an anticancer agent [47,66]. As expected, the DOX:IBU combination with a higher DOX content (5:1 DOX:IBU) displayed the

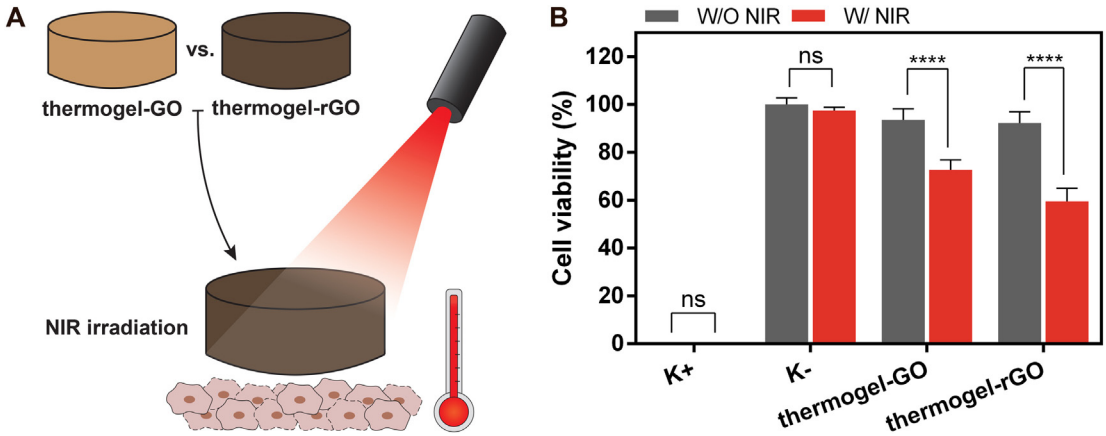

Fig. 4. Schematic representation of the PTT mediated by thermogel-GO and thermogel-rGO (A). Effect of thermogel-GO and thermogel-rGO (at a concentration of 10 μg/mL of GO or rGO) towards MCF-7 cells without (W/O NIR) or with (W/ NIR) NIR laser irradiation (808 nm, 1.7 W/cm^2, 10 min) (B). Data represent mean ± SD, n = 5. (****$p < 0.0001$), ns = non-significant.

lowest half maximal inhibitory concentration (IC_{50}) towards MCF-7 cells (Table S2). Such is in agreement with the fact that the determined IC_{50} of DOX is lower than that of IBU (38.3 μM *vs.* 7738.8 μM; Table S2 and Fig. S5). Subsequently, the combination index (CI) of the different combinations was determined (Fig. S5). Surprisingly, all the DOX:IBU combinations mediated an antagonist effect (CI > 1) on the MCF-7 cells, with the exception of the 1:5 DOX:IBU combination which induced an additive effect (CI = 1) (Fig. S5). The potential of the 1:5 DOX:IBU combination is herein unveiled for the first time, and it is of paramount importance since it enables an optimal combinatorial therapeutic effect using a lower dose of DOX (DOX presents a high off-target toxicity and is costly [67]). In this way, the 1:5 DOX:IBU combination was selected to be incorporated on the thermogel-rGO, yielding thermogel-rGODI.

The thermogel-rGODI displayed an injectability and gelation time-similar to that of thermogel-rGO (Fig. 5A), and its matrix was able to release the loaded drug combination (Fig. S6). Then, the chemo-PTT mediated by the thermogel-rGODI towards MCF-7 cells was investigated (Fig. 5B). For this purpose, cells were incubated with the thermogel-rGODI containing 45.2 or 90.4 μM of the 1:5 DOX:IBU combination (termed as thermogel-rGODI(1x) or thermogel-rGODI(2x), respectively). The MCF-7 cells incubated with thermogel-rGODI(1x) and thermogel-rGODI(2x) suffered a similar reduction on their viability to about 75% (Fig. 5C). These results suggest that the thermogel-rGO matrix may be mediating a controlled delivery of the DOX:IBU combination to cancer cells. However, when NIR light was combined with the thermogel-rGODI(1x), the MCF-7 cells' viability decreased to 49%. An even greater therapeutic effect was mediated by thermogel-rGODI (2x) in combination with NIR light, by further diminishing cells' viability to 34% (Fig. 5C). These results imply that the photothermal heat generated by thermogel-rGODI may sensitize the cancer cells to the therapeutics' action.

In another work, Qiu *et al.* developed agarose-based hydrogels incorporating PEGylated black phosphorus nanostructures and doxorubicin, that could reduce MDA-MB-231 cells' viability to about 35% upon NIR laser irradiation (808 nm, 1 W/cm^2, 10 min; 500 μg/mL of black phosphorus; 344 μM of DOX) [1]. In this work, the chemo-PTT mediated by the thermogel-rGODI(2x) diminished cancer cells' viability to 34% at a slightly higher radiation intensity (808 nm, 1.7 W/cm^2, 10 min) but using a lower dose of therapeutics (90.4 μM of the 1:5 DOX:IBU combination). In this way, thermogel-rGODI is a promising injectable *in situ* forming hydrogel for combinatorial chemo-PTT of breast cancer cells.

4. Conclusions

In this work, injectable chitosan-agarose *in situ* forming thermo-responsive hydrogels incorporating GO and rGO were prepared for

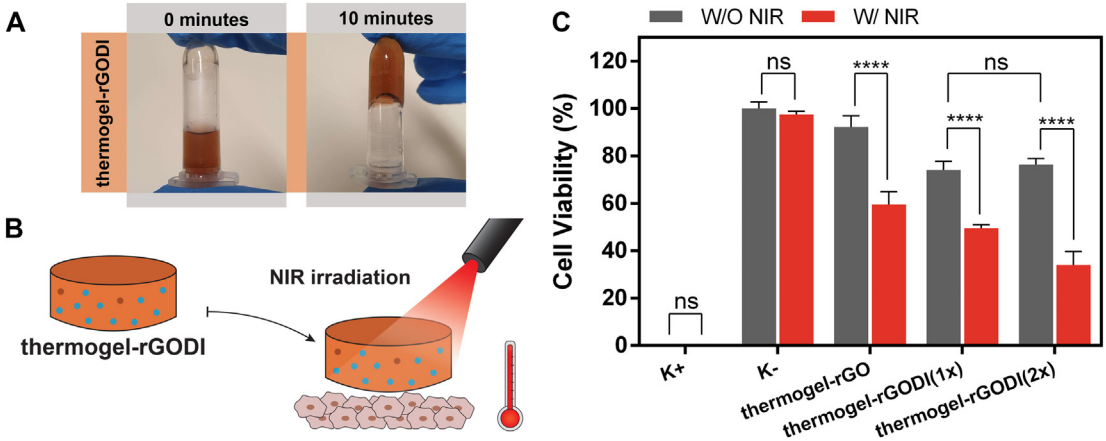

Fig. 5. Evaluation of the combinatorial chemo-PTT mediated by the thermogel-rGODI. Macroscopic images of the thermogel-rGODI gelation (A). Schematic representation of the combinatorial chemo-PTT mediated by the thermogel-rGODI (B). Effect of thermogel-rGODI (10 μg/mL of rGO; 45.2 μM and 90.4 μM of the 1:5 DOX:IBU combination for thermogel-rGODI(1x) and thermogel-rGODI(2x), respectively) against MCF-7 cells without (W/O NIR) or with NIR (W/ NIR) laser irradiation (808 nm, 1.7 W/cm^2, 10 min) (C). Data represent mean ± SD, n = 5. (****$p < 0.0001$), ns = non-significant.

application in cancer therapy. The hydrogels displayed suitable injectability and gelation time as well as good physicochemical properties and cytocompatibility. When irradiated with NIR light, the thermogel-rGO was able to produce a 3.8-times higher temperature increase than thermogel-GO due to the increased photothermal capacity of rGO. Consequently, the PTT mediated by thermogel-rGO could decrease MCF-7 cells' viability to 60% while that generated by thermogel-GO only reduced to 73%. By incorporating an optimized molar ratio of the DOX:IBU combination on the thermogel-rGO, this formulation mediated a chemo-photothermal effect that further diminished MCF-7 cells viability to 34%. The hydrogels' antibacterial activity was also enhanced upon NIR laser irradiation, which is an important feature considering the possible risk of infection at the injection site. Overall, thermogel-rGO is a promising injectable *in situ* forming hydrogel for combinatorial chemo-PTT of breast cancer cells and NIR light enhanced antibacterial applications.

In the future, determining the *in vivo* chemo-PTT effect mediated by the thermogel-rGO and the gel's biodegradability will be crucial to disclose the full therapeutic capacity and safety of this approach. Furthermore, the selectivity of this strategy may be enhanced by functionalizing the rGO nanosheets with targeting ligands while its efficacy can be improved by increasing the rGO content in the formulations. On the other hand, the NIR-enhanced antibacterial properties of thermogel-rGO may be combined with other antibacterial agents (*e.g.* silver nanoparticles), opening a venue for wound healing applications.

Author statement

Rita Lima-Sousa: Conceptualization, Investigation, Formal analysis, Writing - original draft. **Duarte de Melo-Diogo**: Conceptualization, Investigation, Supervision, Writing - review & editing. **Cátia G. Alves**: Investigation. **Cátia S. D. Cabral**: Investigation. **Sónia P. Miguel**: Investigation. **António G. Mendonça**: Supervision, Writing - review & editing. **Ilídio J. Correia**: Project administration, Funding acquisition, Supervision, Writing - review & editing.

Declaration of competing interest

The authors declare that they have no known competing financial interests or personal relationships that could have appeared to influence the work reported in this paper.

Acknowledgments

This work was supported by FEDER funds through the POCI – COMPETE 2020 – Operational Programme Competitiveness and Internationalisation in Axis I – Strengthening research, technological development and innovation (Project POCI-01-0145-FEDER-007491) and National Funds by FCT – Foundation for Science and Technology (Project UID/Multi/00709/2013). The funding from CENTRO-01-0145-FEDER-028989 and POCI-01-0145-FEDER-031462 is also acknowledged. Duarte de Melo-Diogo acknowledges CENTRO-01-0145-FEDER-028989 for the funding given on the form of a research contract. Cátia G. Alves and Rita Lima-Sousa acknowledge funding from the grant UBI-Santander/Totta and individual PhD fellowships from FCT (SFRH/BD/145386/2019 and SFRH/BD/144922/2019).

Appendix A. Supplementary data

Supplementary data to this article can be found online at https://doi.org/10.1016/j.msec.2020.111294.

References

[1] M. Qiu, D. Wang, W. Liang, L. Liu, Y. Zhang, X. Chen, D.K. Sang, C. Xing, Z. Li, B. Dong, F. Xing, D. Fan, S. Bao, H. Zhang, Y. Cao, Novel concept of the smart NIR light–controlled drug release of black phosphorus nanostructure for cancer therapy, Proc. Natl. Acad. Sci. 115 (3) (2018) 501–506.
[2] C. Xing, S. Chen, M. Qiu, X. Liang, Q. Liu, Q. Zou, Z. Li, Z. Xie, D. Wang, B. Dong, L. Liu, D. Fan, H. Zhang, Conceptually novel black phosphorus/cellulose hydrogels as promising photothermal agents for effective cancer therapy, Adv. Healthc. Mater. 7 (7) (2018) 1701510.
[3] M. Luo, T. Fan, Y. Zhou, H. Zhang, L. Mei, 2D black phosphorus–based biomedical applications, Adv. Funct. Mater. 29 (13) (2019) 1808306.
[4] Z. Sun, Y. Zhao, Z. Li, H. Cui, Y. Zhou, W. Li, W. Tao, H. Zhang, H. Wang, P.K. Chu, X.-F. Yu, TiL4-coordinated black phosphorus quantum dots as an efficient contrast agent for in vivo photoacoustic imaging of cancer, Small 13 (11) (2017) 1602896.
[5] M. Qiu, W.X. Ren, T. Jeong, M. Won, G.Y. Park, D.K. Sang, L.-P. Liu, H. Zhang, J.S. Kim, Omnipotent phosphorene: a next-generation, two-dimensional nanoplatform for multidisciplinary biomedical applications, Chem. Soc. Rev. 47 (15) (2018) 5588–5601.
[6] M. Qiu, A. Singh, D. Wang, J. Qu, M. Swihart, H. Zhang, P.N. Prasad, Biocompatible and biodegradable inorganic nanostructures for nanomedicine: silicon and black phosphorus, Nano Today 25 (2019) 135–155.
[7] X. Ji, N. Kong, J. Wang, W. Li, Y. Xiao, S.T. Gan, Y. Zhang, Y. Li, X. Song, Q. Xiong, S. Shi, Z. Li, W. Tao, H. Zhang, L. Mei, J. Shi, A novel top-down synthesis of ultrathin 2D boron nanosheets for multimodal imaging-guided cancer therapy, Adv. Mater. 30 (36) (2018) 1803031.
[8] W. Tao, X. Ji, X. Zhu, L. Li, J. Wang, Y. Zhang, P.E. Saw, W. Li, N. Kong, M.A. Islam, T. Gan, X. Zeng, H. Zhang, M. Mahmoudi, G.J. Tearney, O.C. Farokhzad, Two-dimensional antimonene-based photonic nanomedicine for cancer theranostics, Adv. Mater. 30 (38) (2018) 1802061.
[9] T. Xue, W. Liang, Y. Li, Y. Sun, Y. Xiang, Y. Zhang, Z. Dai, Y. Duo, L. Wu, K. Qi, B.N. Shivananju, L. Zhang, X. Cui, H. Zhang, Q. Bao, Ultrasensitive detection of miRNA with an antimonene-based surface plasmon resonance sensor, Nat. Commun. 10 (28) (2019).
[10] W. Tao, X. Ji, X. Xu, M.A. Islam, Z. Li, S. Chen, P.E. Saw, H. Zhang, Z. Bharwani, Z. Guo, J. Shi, O.C. Farokhzad, Antimonene quantum dots: synthesis and application as near-infrared photothermal agents for effective cancer therapy, Angew. Chem. Int. Ed. 56 (39) (2017) 11896–11900.
[11] C. Xing, S. Chen, X. Liang, Q. Liu, M. Qu, Q. Zou, J. Li, H. Tan, L. Liu, D. Fan, H. Zhang, Two-dimensional MXene (Ti3C2)-integrated cellulose hydrogels: toward smart three-dimensional network nanoplatforms exhibiting light-induced swelling and bimodal photothermal/chemotherapy anticancer activity, ACS Appl. Mater. Interfaces 10 (33) (2018) 27631–27643.
[12] W. Tao, N. Kong, X. Ji, Y. Zhang, A. Sharma, J. Ouyang, B. Qi, J. Wang, N. Xie, C. Kang, H. Zhang, O.C. Farokhzad, J.S. Kim, Emerging two-dimensional monoelemental materials (Xenes) for biomedical applications, Chem. Soc. Rev. 48 (11) (2019) 2891–2912.
[13] K. Yang, L. Feng, X. Shi, Z. Liu, Nano-graphene in biomedicine: theranostic applications, Chem. Soc. Rev. 42 (2) (2013) 530–547.
[14] D. de Melo-Diogo, R. Lima-Sousa, C.G. Alves, E.C. Costa, R.O. Louro, I.J. Correia, Functionalization of graphene family nanomaterials for application in cancer therapy, Colloids Surf. B: Biointerfaces 171 (2018) 260–275.
[15] D. de Melo-Diogo, R. Lima-Sousa, C.G. Alves, I.J. Correia, Graphene family nanomaterials for application in cancer combination photothermal therapy, Biomater. Sci. 7 (9) (2019) 3534–3551.
[16] W. Miao, G. Shim, S. Lee, S. Lee, Y.S. Choe, Y.K. Oh, Safety and tumor tissue accumulation of pegylated graphene oxide nanosheets for co-delivery of anticancer drug and photosensitizer, Biomaterials 34 (13) (2013) 3402–3410.
[17] W. Zhang, Z. Guo, D. Huang, Z. Liu, X. Guo, H. Zhong, Synergistic effect of chemo-photothermal therapy using PEGylated graphene oxide, Biomaterials 32 (33) (2011) 8555–8561.
[18] W. Jiang, F. Mo, Y. Lin, X. Wang, L. Xu, F. Fu, Tumor targeting dual stimuli responsive controllable release nanoplatform based on DNA-conjugated reduced graphene oxide for chemo-photothermal synergetic cancer therapy, J. Mater. Chem. B 6 (26) (2018) 4360–4367.
[19] W. Jiang, F. Mo, X. Jin, L. Chen, L.J. Xu, L. Guo, F. Fu, Tumor-targeting photothermal heating-responsive nanoplatform based on reduced graphene oxide/mesoporous silica/hyaluronic acid nanocomposite for enhanced photodynamic therapy, Adv. Mater. Interfaces 4 (20) (2017) 1700425.
[20] D. de Melo-Diogo, C. Pais-Silva, D.R. Dias, A.F. Moreira, I.J. Correia, Strategies to improve cancer photothermal therapy mediated by nanomaterials, Adv. Healthc. Mater. 6 (10) (2017).
[21] D. de Melo-Diogo, E.C. Costa, C.G. Alves, R. Lima-Sousa, P. Ferreira, R.O. Louro, I.J. Correia, POxylated graphene oxide nanomaterials for combination chemo-phototherapy of breast cancer cells, Eur. J. Pharm. Biopharm. 131 (2018) 162–169.
[22] R. Lima-Sousa, D. de Melo-Diogo, C.G. Alves, E.C. Costa, P. Ferreira, R.O. Louro, I.J. Correia, Hyaluronic acid functionalized green reduced graphene oxide for targeted cancer photothermal therapy, Carbohydr. Polym. 200 (2018) 93–99.
[23] Z. Liu, J.T. Robinson, X. Sun, H. Dai, PEGylated nanographene oxide for delivery of water-insoluble cancer drugs, J. Am. Chem. Soc. 130 (33) (2008) 10876–10877.
[24] K. Yang, S. Zhang, G. Zhang, X. Sun, S.-T. Lee, Z. Liu, Graphene in mice: ultrahigh in vivo tumor uptake and efficient photothermal therapy, Nano Lett. 10 (9) (2010) 3318–3323.
[25] K. Yang, J. Wan, S. Zhang, B. Tian, Y. Zhang, Z. Liu, The influence of surface chemistry and size of nanoscale graphene oxide on photothermal therapy of cancer

using ultra-low laser power, Biomaterials 33 (7) (2012) 2206–2214.
[26] D. de Melo-Diogo, C. Pais-Silva, E.C. Costa, R.O. Louro, I.J. Correia, D-alpha-tocopheryl polyethylene glycol 1000 succinate functionalized nanographene oxide for cancer therapy, Nanomedicine (London, England) 12 (5) (2017) 443–456.
[27] H.-J. Im, C.G. England, L. Feng, S.A. Graves, R. Hernandez, R.J. Nickles, Z. Liu, D.S. Lee, S.Y. Cho, W. Cai, Accelerated blood clearance phenomenon reduces the passive targeting of PEGylated nanoparticles in peripheral arterial disease, ACS Appl. Mater. Interfaces 8 (28) (2016) 17955–17963.
[28] S. Wilhelm, A.J. Tavares, Q. Dai, S. Ohta, J. Audet, H.F. Dvorak, W.C.W. Chan, Analysis of nanoparticle delivery to tumours, Nat. Rev. Mater. 1 (5) (2016) 16014.
[29] J.C. Boga, S.P. Miguel, D. de Melo-Diogo, A.G. Mendonca, R.O. Louro, I.J. Correia, In vitro characterization of 3D printed scaffolds aimed at bone tissue regeneration, Colloids Surf. B: Biointerfaces 165 (2018) 207–218.
[30] C.S.D. Cabral, S.P. Miguel, D. de Melo-Diogo, R.O. Louro, I.J. Correia, Green reduced graphene oxide functionalized 3D printed scaffolds for bone tissue regeneration, Carbon 146 (2019) 513–523.
[31] E. Piantanida, G. Alonci, A. Bertucci, L. De Cola, Design of nanocomposite injectable hydrogels for minimally invasive surgery, Acc. Chem. Res. 52 (8) (2019) 2101–2112.
[32] D.-Y. Fan, Y. Tian, Z.-J. Liu, Injectable hydrogels for localized cancer therapy, Front. Chem. (Lausanne, Switzerland) 7 (675) (2019).
[33] P. Davoodi, W.C. Ng, W.C. Yan, M.P. Srinivasan, C.-H. Wang, Double-walled microparticles-embedded self-cross-linked, injectable, and antibacterial hydrogel for controlled and sustained release of chemotherapeutic agents, ACS Appl. Mater. Interfaces 8 (35) (2016) 22785–22800.
[34] Y.T. Fong, C.H. Chen, J.P. Chen, Intratumoral delivery of doxorubicin on folate-conjugated graphene oxide by in-situ forming thermo-sensitive hydrogel for breast cancer therapy, Nanomaterials 7 (11) (2017).
[35] X. Zhu, H. Zhang, H. Huang, Y. Zhang, L. Hou, Z. Zhang, Functionalized graphene oxide-based thermosensitive hydrogel for magnetic hyperthermia therapy on tumors, Nanotechnology 26 (36) (2015) 365103.
[36] H. Tan, K.G. Marra, Injectable, biodegradable hydrogels for tissue engineering applications, Materials 3 (3) (2010) 1746–1767.
[37] L. Klouda, A.G. Mikos, Thermoresponsive hydrogels in biomedical applications, Eur. J. Pharm. Biopharm. 68 (1) (2008) 34–45.
[38] S.P. Miguel, M.P. Ribeiro, H. Brancal, P. Coutinho, I.J. Correia, Thermoresponsive chitosan-agarose hydrogel for skin regeneration, Carbohydr. Polym. 111 (2014) 366–373.
[39] A. Hmed, A. Sofy, A. Sharaf, K. El Dougdoug, Effectiveness of chitosan as naturally-derived antimicrobial to fulfill the needs of today's consumers looking for food without hazards of chemical preservatives, J. Microbiol. Res. 7 (2017) 55–67.
[40] D.R. Perinelli, L. Fagioli, R. Campana, J.K.W. Lam, W. Baffone, G.F. Palmieri, L. Casettari, G. Bonacucina, Chitosan-based nanosystems and their exploited antimicrobial activity, Eur. J. Pharm. Sci. 117 (2018) 8–20.
[41] E. Fernández, D. López, C. Mijangos, M. Duskova-Smrckova, M. Ilavsky, K. Dusek, Rheological and thermal properties of agarose aqueous solutions and hydrogels, J. Polym. Sci. B Polym. Phys. 46 (3) (2008) 322–328.
[42] H.-F. Ko, C. Sfeir, P.N. Kumta, Novel synthesis strategies for natural polymer and composite biomaterials as potential scaffolds for tissue engineering, Philos. Trans. R. Soc. A Math. Phys. Eng. Sci. 368 (1917) (2010) 1981–1997.
[43] C. Wu, J. Zhao, F. Hu, Y. Zheng, H. Yang, S. Pan, S. Shi, X. Chen, S. Wang, Design of injectable agar-based composite hydrogel for multi-mode tumor therapy, Carbohydr. Polym. (2018) 112–121.
[44] P.C. Pires, D. Peixoto, I. Teixeira, M. Rodrigues, G. Alves, A.O. Santos, Nanoemulsions and thermosensitive nanoemulgels of phenytoin and fosphenytoin for intranasal administration: formulation development and in vitro characterization, Eur. J. Pharm. Sci. 141 (2020) 105099.
[45] V.M. Gaspar, P. Baril, E.C. Costa, D. de Melo-Diogo, F. Foucher, J.A. Queiroz, F. Sousa, C. Pichon, I.J. Correia, Bioreducible poly(2-ethyl-2-oxazoline)-PLA-PEI-SS triblock copolymer micelles for co-delivery of DNA minicircles and Doxorubicin, J. Control. Release 213 (2015) 175–191.
[46] C.G. Alves, D. de Melo-Diogo, R. Lima-Sousa, E.C. Costa, I.J. Correia, Hyaluronic acid functionalized nanoparticles loaded with IR780 and DOX for cancer chemo-photothermal therapy, Eur. J. Pharm. Biopharm. 137 (2019) 86–94.
[47] A.F. Moreira, V.M. Gaspar, E.C. Costa, D. de Melo-Diogo, P. Machado, C.M. Paquete, I.J. Correia, Preparation of end-capped pH-sensitive mesoporous silica nanocarriers for on-demand drug delivery, Eur. J. Pharm. Biopharm. 88 (3) (2014) 1012–1025.
[48] N. Chirani, L.H. Yahia, L. Gritsch, F. Motta, S. Chirani, S. Farè, History and applications of hydrogels, J. Biomed. Sci. 4 (2015) 13–23.
[49] R. Dong, X. Zhao, B. Guo, P.X. Ma, Self-healing conductive injectable hydrogels with antibacterial activity as cell delivery carrier for cardiac cell therapy, ACS Appl. Mater. Interfaces 8 (27) (2016) 17138–17150.
[50] Y.P. Singh, N. Bhardwaj, B.B. Mandal, Potential of agarose/silk fibroin blended hydrogel for in vitro cartilage tissue engineering, ACS Appl. Mater. Interfaces 8 (33) (2016) 21236–21249.
[51] L. Saeednia, L. Yao, K. Cluff, R. Asmatulu, Sustained releasing of methotrexate from injectable and thermosensitive chitosan–carbon nanotube hybrid hydrogels effectively controls tumor cell growth, ACS Omega 4 (2) (2019) 4040–4048.
[52] L. Saeednia, L. Yao, M. Berndt, K. Cluff, R. Asmatulu, Structural and biological properties of thermosensitive chitosan–graphene hybrid hydrogels for sustained drug delivery applications, J. Biomed. Mater. Res. A 105 (9) (2017) 2381–2390.
[53] M.V. Ghica, M. Hîrjău, D. Lupuleasa, C.E. Dinu-Pîrvu, Flow and thixotropic parameters for rheological characterization of hydrogels, Molecules (Basel, Switzerland) 21 (6) (2016) 786.
[54] J.P. Chaudhary, D.R. Chejara, D. Makwana, K. Prasad, R. Meena, Agarose based multifunctional materials: evaluation of thixotropy, self-healability and stretchability, Carbohydr. Polym. 114 (2014) 306–311.
[55] R. Xing, K. Liu, T. Jiao, N. Zhang, K. Ma, R. Zhang, Q. Zou, G. Ma, X. Yan, An injectable self-assembling collagen–gold hybrid hydrogel for combinatorial antitumor photothermal/photodynamic therapy, Adv. Mater. 28 (19) (2016) 3669–3676.
[56] K.F. Chu, D.E. Dupuy, Thermal ablation of tumours: biological mechanisms and advances in therapy, Nat. Rev. Cancer 14 (3) (2014) 199–208.
[57] L. Cheng, C. Wang, L. Feng, K. Yang, Z. Liu, Functional nanomaterials for phototherapies of cancer, Chem. Rev. 114 (21) (2014) 10869–10939.
[58] Y.-W. Jiang, G. Gao, P. Hu, J.-B. Liu, Y. Guo, X. Zhang, X.-W. Yu, F.-G. Wu, X. Lu, Palladium nanosheet-knotted injectable hydrogels formed via palladium–sulfur bonding for synergistic chemo-photothermal therapy, Nanoscale 12 (1) (2020) 210–219.
[59] D. Simões, S.P. Miguel, M.P. Ribeiro, P. Coutinho, A.G. Mendonça, I.J. Correia, Recent advances on antimicrobial wound dressing: a review, Eur. J. Pharm. Biopharm. 127 (2018) 130–141.
[60] D. Raafat, H.-G. Sahl, Chitosan and its antimicrobial potential—a critical literature survey, Microb. Biotechnol. 2 (2) (2009) 186–201.
[61] A.F. Moreira, C.F. Rodrigues, T.A. Jacinto, S.P. Miguel, E.C. Costa, I.J. Correia, Poly (vinyl alcohol)/chitosan layer-by-layer microneedles for cancer chemo-photothermal therapy, Int. J. Pharm. 576 (2020) 118907.
[62] T.A. Jacinto, C.F. Rodrigues, A.F. Moreira, S.P. Miguel, E.C. Costa, P. Ferreira, I.J. Correia, Hyaluronic acid and vitamin E polyethylene glycol succinate functionalized gold-core silica shell nanorods for cancer targeted photothermal therapy, Colloids Surf. B: Biointerfaces 188 (2020) 110778.
[63] H.H. Duong, L.Y. Yung, Synergistic co-delivery of doxorubicin and paclitaxel using multi-functional micelles for cancer treatment, Int. J. Pharm. (Amsterdam, Netherlands) 454 (1) (2013) 486–495.
[64] G. Babos, E. Biro, M. Meiczinger, T. Feczko, Dual drug delivery of sorafenib and doxorubicin from PLGA and PEG-PLGA polymeric nanoparticles, Polymers 10 (8) (2018).
[65] K. Li, W. Zhan, Y. Chen, R.K. Jha, X. Chen, Docetaxel and doxorubicin codelivery by nanocarriers for synergistic treatment of prostate cancer, Front. Pharmacol. 10 (2019) 1436.
[66] J.G. Marques, V.M. Gaspar, E. Costa, C.M. Paquete, I.J. Correia, Synthesis and characterization of micelles as carriers of non-steroidal anti-inflammatory drugs (NSAID) for application in breast cancer therapy, Colloids Surf. B: Biointerfaces 113 (2014) 375–383.
[67] L.M. Kaminskas, V.M. McLeod, B.D. Kelly, G. Sberna, B.J. Boyd, M. Williamson, D.J. Owen, C.J.H. Porter, A comparison of changes to doxorubicin pharmacokinetics, antitumor activity, and toxicity mediated by PEGylated dendrimer and PEGylated liposome drug delivery systems, Nanomedicine 8 (1) (2012) 103–111.